

A ROBUST ROBOTIC HAND FOR UNSTRUCTURED ENVIRONMENTS

Aaron M. Dollar, Harvard University

INTRODUCTION

One of the central challenges of robotics is grasping and manipulating objects in unstructured environments, where object properties are not known *a priori* and sensing is prone to error. The resulting uncertainty in the relationship between the object and gripper makes it difficult to control contact forces and establish a successful grasp.

One approach to dealing with this uncertainty is through compliance, so that positioning errors do not result in large forces and the grasper conforms to the object. Compliance has most often been implemented through control of manipulator impedance, based on active use of joint sensors for position, velocity and force/torque [1]. However, carefully designed *mechanical* compliance in the finger structure can allow the gripper to passively conform to a wide range of objects while minimizing contact forces.

Along these lines, I have designed and built a particularly robust robotic hand with passively compliant joints (Fig. 1). The hand was fabricated using polymer-based Shape Deposition Manufacturing (SDM) [2], a new layered manufacturing technique with which the rigid links and compliant joints of the gripper are created simultaneously, with embedded sensing and actuation components. The result is an extremely robust gripper. Elastomeric flexures create compliant joints, eliminating metal bearings, and tough rigid polymers fully encase the embedded components, eliminating the need for seams and fasteners that are often the source of mechanical failure. The hand adapts to large uncertainties in object position and properties, and is fully functional after impacts and other large loads due to the unintended contact that is likely to occur in unstructured tasks.

HAND DESIGN AND FABRICATION

Fig. 2 diagrams the parts of the SDM finger. The concave side of each link contains a soft fingerpad to maximize friction and increase grasp stability [3,4]. Links are connected via viscoelastic joint flexures, designed to be compliant in the plane of finger motion and stiff out of plane. Fig. 3 shows the behavior of the distal finger joint through its range of motion.

The link lengths, measured from the centers of the joint flexures, were chosen to be equal to enable the tip to reach the origin. The joint rest angles and joint stiffnesses of the fingers were chosen based on optimization studies presented later in this document. The design is almost completely 2.5 dimensional (i.e. extruded 2 dimensional shapes), allowing for the same finger to be used on the right or left side of the grasper.

Due to the molding process used to create them, the SDM fingers, with embedded sensors and actuation components, consist as a single part (weighing 39 grams), with no fasteners



Fig. 1. Four-fingered SDM hand with support blocks to prevent joint creep when not in use. Actuators are not attached to the hand in this image.

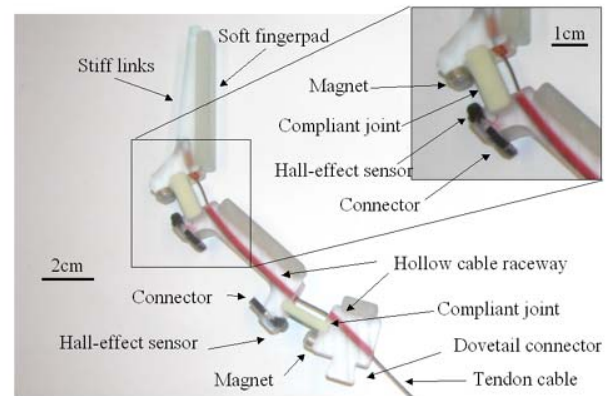


Fig. 2. Details of finger parts and placement of components.

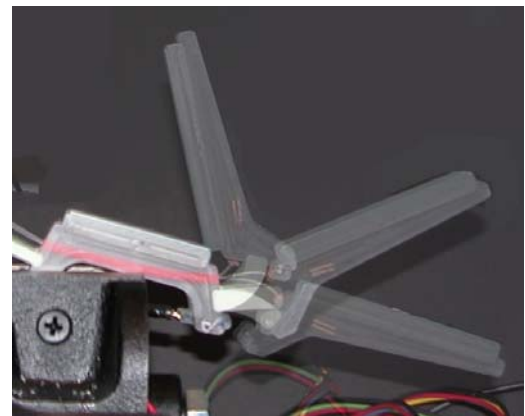


Fig. 3 Superimposed photograph of joint deflection and link motion for three positions across the travel range of the distal joint of the fingers. The center image is the rest position.

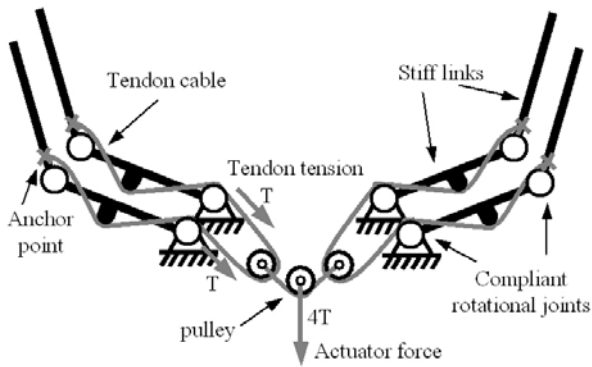


Fig. 4 Actuation schematic of the hand

or adhesives! This is in stark contrast to a similar conventionally-assembled grasper used in previous work (60 parts total, 40 fasteners, weighing 200 grams).

For actuation, each finger has a pre-stretched, nylon-coated stainless steel cable anchored into the distal link, and running through low-friction nylon 11 tubing to the base. The grasper is intended to be unactuated until contact is made with the target object and a successful grasp is predicted based on the available sensory information. Before actuation, the tendon cable, which is in parallel with the compliant joints, remains slack, and the finger is in its most compliant state. This method permits the use of actuators that are not backdrivable and prevents the inertial load of the actuator from increasing the passive stiffness. After actuation, the stiff tendon takes much of the compliance out of the fingers, resulting in a grasp with greater stability.

The gripper is driven by a single actuator for the four fingers. This property not only makes the gripper simpler and lighter, but it also allows the gripper to be self-adaptable to the target object. Fig. 4 details the actuation scheme, by which motion of the distal links can continue after contact on the coupled proximal links occurs, allowing the finger to passively adapt to the object shape. Additionally, the pulley design in this scheme allows the remaining fingers to continue to enclose the object after the other fingers have been immobilized by contact, ensuring that each tendon cable shares an equal amount of tension. The details of the joint coupling scheme employed on each finger are presented in the “design procedure” section of this document.

Although not described in detail here, each joint contains a high-resolution joint angle sensor built by embedding a low output impedance linear hall-effect sensor on one side of the joint and a rare-earth magnet on the other (Fig. 2). Joint motion changes the distance between the two, varying the sensor output. Also, a piezo-film strip is embedded within the proximal finger pad to create a low-threshold contact sensor (not shown).

The polyurethane used for these joints demonstrates significant viscoelastic behavior, which is necessary to reduce the severity of joint oscillations and permit the use of low joint stiffness. Figure 5 shows the joint response of the SDM finger to a large step displacement of the fingertip, released at time $t=0$. Note that the oscillations are negligible after less than 1

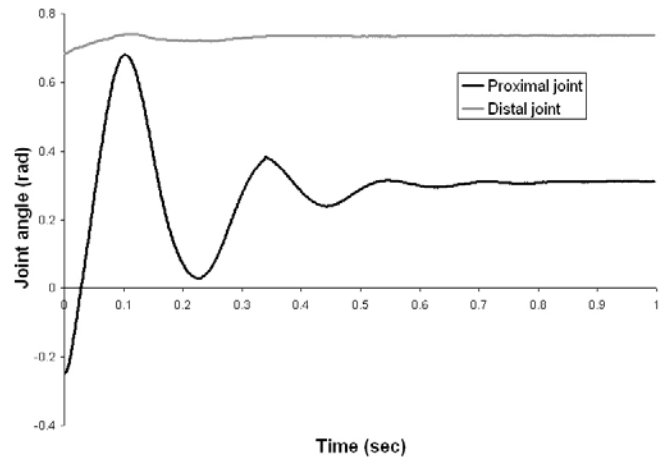


Fig. 5 Joint response of the SDM finger to a tip step displacement released at time=0.

second. In a conventionally-assembled grasper, oscillations due to large step displacements were found to persist for tens of seconds after release.

The viscoelastic properties of this material were found to be consistent with a second-order Kelvin model [5] with fit

$$k_{\theta} = 0.176 + 0.0303e^{-0.0156t} + 0.0437e^{-0.00125t}, \quad (1)$$

where k_{θ} and t have units of (Nm/rad, seconds), respectively. The time constants are much larger than typical grasp time, so the damping in the material has little effect on control of the grasper. While these experimental results are not shown here, the basic shape of this curve can be seen as the envelope of the curves in Fig. 5.

SDM FABRICATION PROCEDURE

The diagram in Fig. 6 shows the steps of the SDM process used to produce the compliant grasper fingers. Pockets corresponding to the shape of the stiff links of our fingers are machined into a high-grade machine wax. The components in panel A are put into place in the pockets (panel B), and the polymer resin poured. Modeling clay is used to dam any areas to be blocked from the resin. After the layer cures, a second group of pockets is machined (both into the support wax and the stiff resin) and dammed (panel C). The polymer resins for the compliant finger joints and soft fingerpads are then poured (panel D) and allowed to cure. The block is then faced off to level the surface and remove surface flaws (panel E), and the completed fingers removed from the wax support material. The entire process takes approximately 30 hours to complete, only 4 of which require human intervention.

DESIGN PROCEDURE

In order to determine the best compliance, kinematic, and joint coupling configuration for the hand, I constructed a series of simulations to model how variations in these parameters affect the ability to grasp objects in the presence of uncertainty. Performance was compared on the basis of the maximum range of object size and location that could be successfully grasped and the magnitude of contact forces.

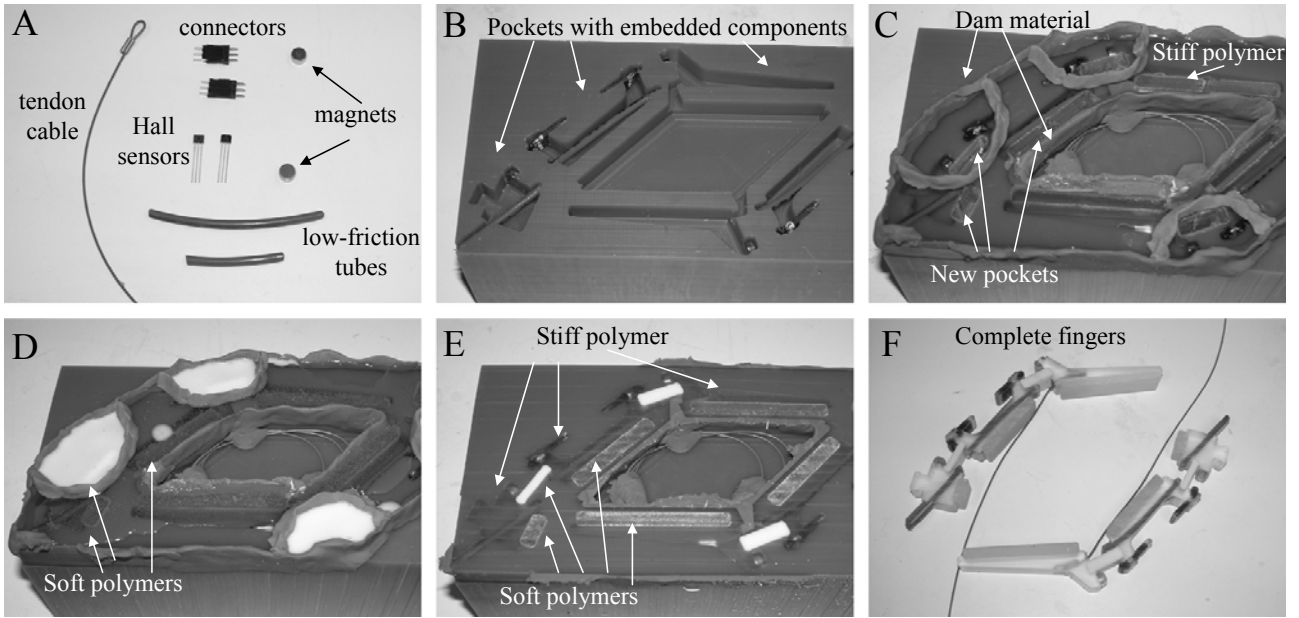


Fig. 6 Steps of the Shape Deposition Manufacturing (SDM) process used to fabricate the grasper fingers.

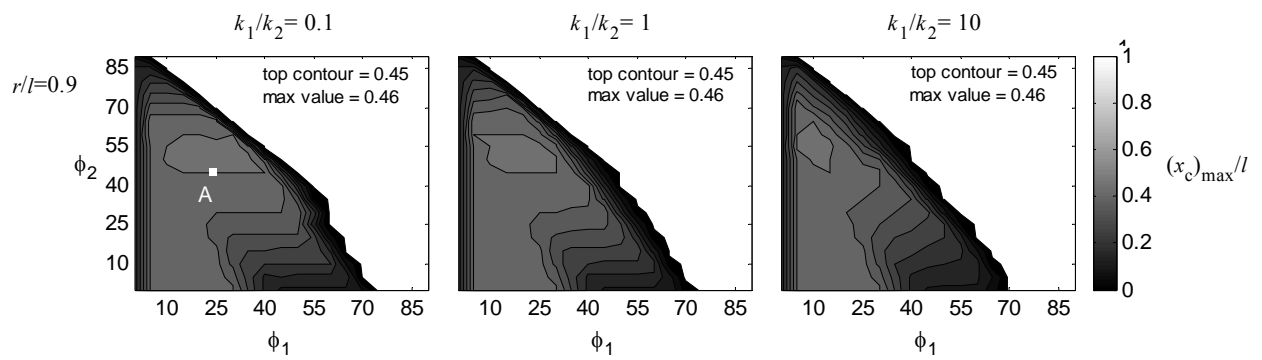


Fig. 7 Successful grasp range as rest angle and stiffness ratio are varied for a large object.

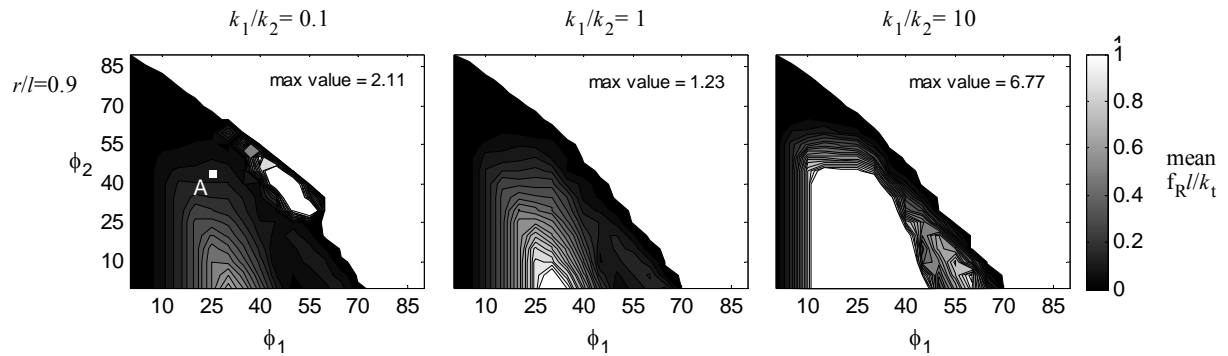


Fig. 8 Average contact force as rest angle and stiffness ratio are varied for a large object.

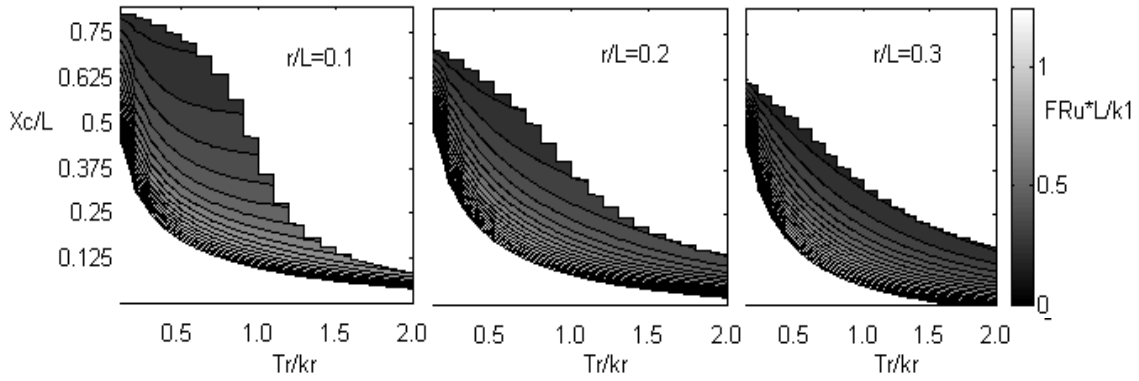


Fig. 9. Unbalanced object force (F_{Ru}) as object location (x_c/l) and size (r/l) are varied for a range of torque ratio values (τ_r/k_r).

In order to reduce the parameter space and allow for detailed analysis of parametric trade-offs, a simplified version of the gripper is examined: a planar, two-fingered gripper with links that are rigid lines between compliant rotational joints. The object to be grasped was assumed to be circular (a frequent assumption in the grasping literature, and a reasonable approximation for many objects), and sufficiently massive such that the gripper contact forces do not displace or rotate it. A grasp is judged successful if the fingers envelop the object (enclose more than 180° of the object surface). I ignore inertial effects and assume quasi-static conditions.

The models were built using a combination of the inverse kinematics of the mechanism, torque balances for each joint, work balance, and equations describing the geometry of the grasper and object. MATLAB was used to numerically solve these systems of equations and allow for the performance of the grasper to be tested over a wide range of variations in grasper parameters. The details of the model and simulations used to conduct the following optimization studies are not presented here for lack of space.

Two stages of the grasping process were simulated – passive contact with the object before actuation (to optimize grasper preshape and joint stiffness), and grasper behavior and contact forces after actuation (to optimize the joint coupling scheme necessary for underactuation).

Grasper preshape and joint stiffness

In this simulation, the joint rest angles and joint stiffness ratio of the fingers were varied and the performance analyzed to maximize the allowable uncertainty in object location (successful grasp range) and size as well as minimize contact forces. Fig. 7 shows a portion of results of the first simulation. The three plots represent three tested proximal/distal joint stiffness ratios. For each plot, the axes are the rest angle for link 1 (ϕ_1 – angle with the horizontal) and link 2 (ϕ_2 – angle with link 1). The contours correspond to the successful grasp range, $(x_c)_{max}$, for each rest angle configuration, normalized by the link length.

The results show that increasing the stiffness ratio (k_1/k_2) does not affect the maximum value of the successful grasp range, $(x_c)_{max}$, but does, however, slightly affect the size of the optimum region. While not shown here, this optimum region for a large object radius ($r/l=0.9$) falls within the optimum

regions for smaller objects.

Fig. 8 shows the results of the force investigation. The contours correspond to the values of the average normalized force (mean f_R/k_T) for each rest angle configuration. These results show that to decrease unwanted contact forces, the proximal joint should be more compliant than the distal joint.

A comparison with Fig. 7 shows that the configurations with the largest successful grasp range also exhibit low average contact force. Taking these results and others not presented here into consideration, the configuration labeled ‘A’ in these two plots ($\phi_1, \phi_2=25, 45^\circ$) was chosen for the final finger design.

These results were confirmed in hardware by testing the performance of a specially-made reconfigurable aluminum grasper as joint rest angles and stiffnesses were varied. A portion of those results are presented later.

Joint coupling scheme

In this simulation, the joint coupling scheme (ratio of torque applied at the proximal/distal joints) was varied in order to maximize the allowable uncertainty in object location (successful grasp range) and size as well as minimize contact forces. Fig. 9 shows a portion of the results of maximum unbalanced object force (F_{Ru}) as object position (x_c/l) and torque ratio (τ_r/k_r) were varied for three small objects ($r/l=0.1, 0.2, 0.3$). Note that the white portions in the upper right of each plot are unsuccessful configurations (no grasp could be achieved), whereas the white areas in the lower left are regions of large F_{Ru} .

These results suggest that, to keep unbalanced object forces low, torque ratio (τ_r/k_r) should be as large as possible. However, as torque ratios (τ_r/k_r) increase, the position range in which an object can be successfully grasped ($\max(x_c/l)$) is decreased. This range ($\max(x_c/l)$) is the outer boundary of the contour plots in Fig. 9.

This tradeoff in force versus successful grasp range can be weighed by considering the quality of the sensory information available for the grasping task. For a task in which the location of the target object is well known, the torque ratio can be large, since the gripper can be reliably centered on the object. However, for tasks in which sensory information is poor, the positioning of the gripper is subject to large errors, requiring that the chosen torque ratio should allow for positions far from

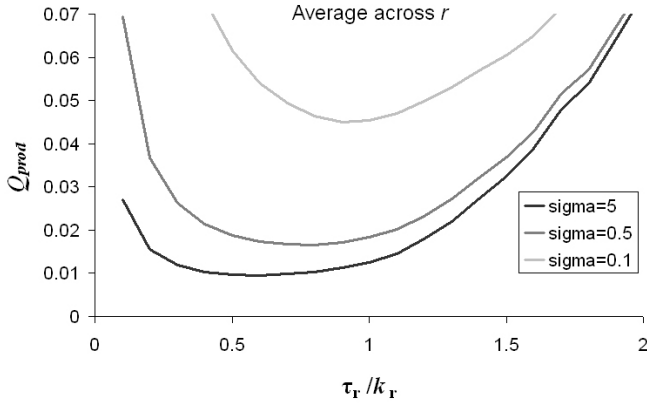


Fig. 10. Total quality averaged across object radius, r/l .

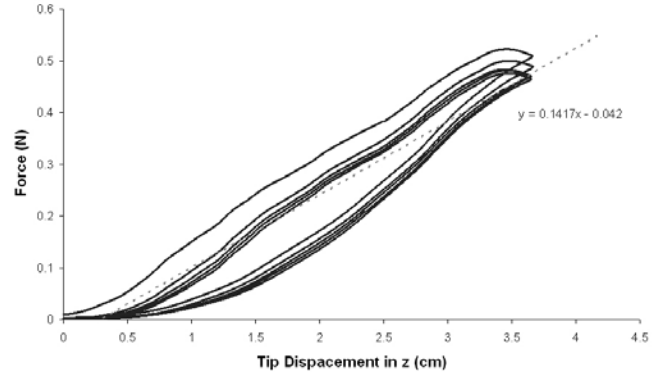


Fig. 11 Force-deflection curve of the tip of the SDM finger with linear trendline. The data represents five cycles of tip motion.

the centerline (x_c/l).

The results of Fig. 9 are further analyzed by weighting the individual data points by a normal distribution of the target object position, x_c/l , for a number of values of standard deviation. Different values of standard deviation of x_c/l correspond to different qualities of sensory information about the object prior to contact (e.g. vision) – large standard deviation corresponding to poor sensing and small standard deviation corresponding to good sensing.

Weighting functions were generated according to the normal, Gaussian distribution (for a mean of zero)

$$y(x) = \frac{1}{\sigma\sqrt{2\pi}} e^{-\frac{x^2}{2\sigma^2}}$$

with normal probability density of

$$p(x) = \int y(x)dx,$$

where $x = x_c/l$.

The normal distribution function was used to calculate a weighted average ($Q_{F_{Ru}}$) of the maximum unbalanced object force over the range of object positions (x_c/l) for a given torque ratio (τ_r/k_r)

$$Q_{F_{Ru}}(\tau_r/k_r) = \sum_i \tilde{F}_{Ru}(\tau_r/k_r, i)$$

$$\text{where } \tilde{F}_{Ru}(\tau_r/k_r, x_c/l) = \frac{F_{Ru}(\tau_r/k_r, x_c/l)y(x_c/l)}{\sum_i y(x_c/l)_i}$$

To address the tradeoff that high torque ratio leads to low grasp range, the normal probability density function was used to calculate a quality measure of the successful grasp range ($Q_{x_{cmax}}$) for a given torque ratio (τ_r/k_r)

$$Q_{x_{cmax}}(\tau_r/k_r) = \left(\frac{x_{cmax}(\tau_r/k_r)p(x_{cmax}(\tau_r/k_r))}{\sum_i p(x_{cmax}(\tau_r/k_r))_i} \right)^{-1}$$

The inversion of the grasp space quality measure serves to allow for comparison with the unbalanced force quality measure – a lower value represents a more desirable configuration. Without the inversion, this term represented the probability that a given torque ratio configuration will be able to successfully grasp an object with the specified position distribution.

In order to provide a quantified sense of the tradeoffs between minimizing force and maximizing grasp space, the product of the two quality measures can be analyzed:

$$Q_{prod}(\tau_r/k_r) = \frac{Q_{F_{Ru}}(\tau_r/k_r)Q_{x_{cmax}}(\tau_r/k_r)}{\sum_i Q_{x_{cmax}}(i)}$$

By calculating a total quality measure in this specific way, we are using the grasp space quality measure as a weighting function on the force quality. In this scheme, all weighting functions are based on the normal distribution of object position.

Fig. 10 shows Q_{prod} as an average over all tested object sizes ($r/l=0.1, 0.2, \dots, 0.9$) for three different standard deviations ($\sigma=5, 0.5, 0.1$). For a large standard deviation in object position (poor sensing), there is a clear optimum at around $(\tau_r/k_r) = 0.6$, and as the standard deviation is lowered (better sensing), this optimum shifts towards $\tau_r/k_r = 1.0$. Since my grasper is intended for unstructured tasks, the results from the large standard deviation weighting are more relevant, and I therefore chose a joint coupling ratio of 0.6 distal/proximal.

TESTING AND EVALUATION

Finger compliance and robustness

Fig. 11 shows the force generated at the tip of the fingers due to displacement in the out-of-plane direction (z direction)

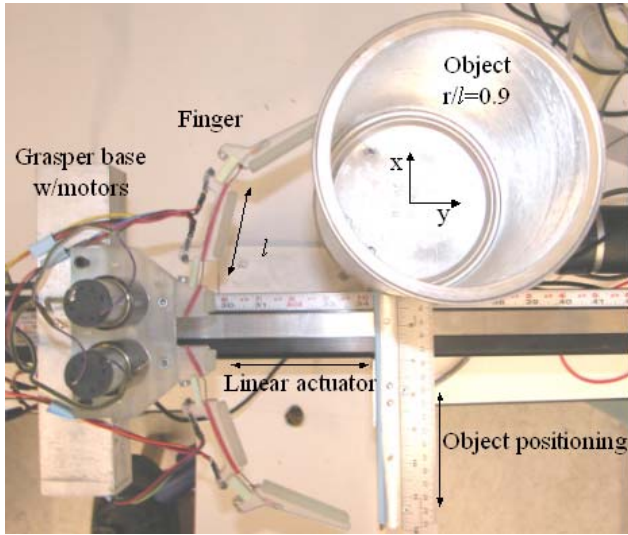


Fig. 12. Experimental setup. The grasper is mounted on an actuated linear slider and the object, affixed to a six-axis force/torque sensor, can be positioned at distances normal to the actuation direction.

following the convention of Fig. 12). The tip was displaced at a rate of approximately 1 cm/sec while mounted on an actuated linear slide mechanism, with force measured by a multi-axis force/torque sensor. This data represents force generated due to motion of the tip across the tested range and back for a total of five cycles, low-pass filtered with a cut-off frequency of 1 Hz, to remove sensor noise. Note the hysteresis in the curves and the force relaxation due to viscoelasticity.

This result shows that the SDM fingers, while exhibiting very low tip stiffness, can also undergo large deflections while remaining completely functional. In the test shown in Fig. 11, the tip was displaced more than 3.5 cm in the out-of-plane direction (approximately 20 degrees) without any degradation of mechanical properties. The advantages of this property are clear when considering the usual result of unplanned contact during use of traditional research robotic hands.

To give a sense of the robustness of the mechanism to impact loads, a more informal test was performed. An SDM finger was repeatedly dropped from a height of over 15m (50') onto a stone floor. After two attempts, no noticeable damage had occurred. After three, a small piece broke off of the dovetail connector. After six attempts, the outer link developed a large crack and one of the magnets broke off – but the sensors and joints remained intact and functional.

Hand performance

In order to test the performance of the SDM hand against the simulation results, the grasper was mounted on a precision screw-driven linear positioner, which brought the grasper into contact with the target object. The objects were positioned at increasing distances x_c from the center of the grasper in the lateral x direction, and securely mounted to prevent motion due to gripper-object contact forces. A diagram of the experimental apparatus is shown in Fig. 12. The objects were metal cylinders chosen to reflect the sizes used in the simulation. Note that the hand used in this study is a planar version of the hand shown in

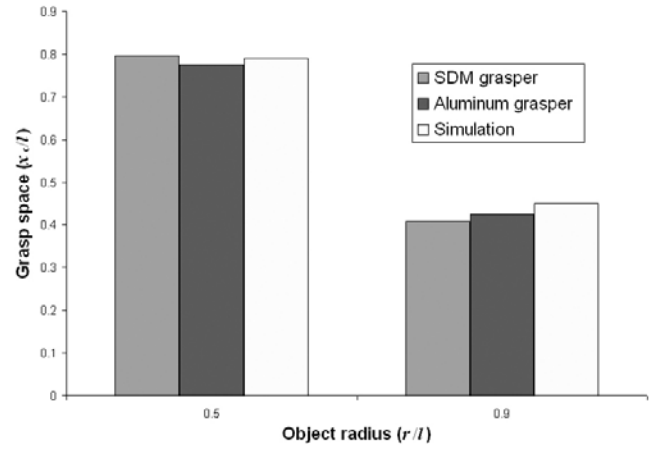


Fig. 13 Successful grasp range of the SDM grasper compared to the aluminum grasper and simulation.

Fig. 1.

Fig. 13 shows the successful grasp range of this SDM grasper and the analogous results from the aluminium grasper and simulation for objects of radius $r/l=0.5$ and 0.9 . The object can be successfully grasped anywhere within this range, indicating the allowable uncertainty in object position for a successful grasp. The results show that the center of an object of radius $r/l=0.5$ can be located anywhere within the range $x_c/l=\pm 0.80$ from the centerline of the grasper. Similarly, a large object ($r/l=0.9$) can be located anywhere within the range $x_c/l=\pm 0.41$. The values of the SDM grasp range show good agreement with the aluminum and simulated graspers.

The full, four-fingered version of the SDM hand is currently undergoing exhaustive testing.

ACKNOWLEDGMENT

I would like to thank Professor Robert D. Howe for his guidance throughout this project, as well as Professor Mark Cutkosky and his students for their advice on implementing the SDM process.

REFERENCES

- [1] K. J. Salisbury, "Active stiffness control of a manipulator in Cartesian coordinates," 19th IEEE Conf. Decision and Control, pp.95-100, 1980.
- [2] R. Merz, F. B. Prinz, K. Ramaswami, M. Terk, L. Weiss, "Shape Deposition Manufacturing," *Proceedings of the Solid Freeform Fabrication Symposium*, University of Texas at Austin, August 8-10, 1994.
- [3] K. B. Shimoga, A. A. Goldenberg, "Soft materials for robotic fingers," *Proceedings of the 1992 IEEE International Conference on Robotics and Automation*, pp. 1300-1305, 1992.
- [4] M. R. Cutkosky, J. M. Jourdain, P. K. Wright, "Skin materials for robotic fingers," *Proceedings of the 1987 IEEE International Conference on Robotics and Automation*, pp. 1649-1654, 1987.
- [5] Y. C. Fung, "Biomechanics: Mechanical properties of living tissues," Springer-Verlag, 2nd edition, 1993.